DISCRETE AND CONTINUOUS
DYNAMICAL SYSTEMS–SERIES B
Volume **6**, Number **2**, March **2006**

Website: http://AIMsciences.org

pp. **339–356**

ALIGNMENT AND RHEO-OSCILLATOR CRITERIA FOR SHEARED NEMATIC POLYMER FILMS IN THE MONOLAYER LIMIT

Joo Hee Lee and M. Gregory Forest

Department of Mathematics
Institute for Advanced Materials, Nanoscience & Technology
University of North Carolina-Chapel Hill
Chapel Hill, NC 27599-3250, USA

Ruhai Zhou

Department of Mathematics and Statistics
Old Dominion University
Norfolk, VA 23529,USA

Abstract. Monolayer films of liquid crystalline polymers (LCPs) are modelled with a mesoscopic two-dimensional (2D) analogue of the Doi-Hess (1981, 1976) rigid rod model. One aim is to establish a more complete solution to the classical problem of how orientational degeneracy of quiescent nematic equilibria breaks in weak shear. We exploit the simplicity of 2D liquids to extend results of Kuzuu and Doi (1983,1984), Marrucci and Maffetone (1989-1991), See, Doi and Larson (1990), Forest *et al.* (2003-2004). We recall the distinction between two versus three dimensional quiescent phase diagrams and the isotropic-nematic phase transition, then analyze the deformation of these respective bifurcation diagrams in shear flow. We give a simple proof that limit cycles, known as tumbling orbits, must arise beyond the parameter boundary for the steady-unsteady transition. Finally, we show the shear-perturbed 2D phase diagram is significantly more robust to closure approximations than the 3D system.

1. **Introduction.** Hess [13] and Doi [4] proposed the nematic liquid crystalline model which provides an evolution equation for the orientational probability density function of rod-like molecules in a laminar flow field. Marrucci and Maffetonne developed an insightful analysis of the two-dimensional form of this model to understand the steady-unsteady transition in weak shear [22]. For the case of two-dimensional nematic polymers, Maffetonne and Crescitelli [18, 19] analyzed a simplified constitutive equation in order to examine closure approximations and numerically explored bifurcations of the kinetic model equation using the continuation software AUTO [3, 5]. These model predictions were applied to experiments on monolayers of nematic polymers performed in Fuller's group [21, 28]. Faraoni and Grosso *et al.* [6], following initial results of Larson and Öttinger [17], revealed

2000 *Mathematics Subject Classification.* 76A15, 82D60.

Key words and phrases. Liquid crystal polymers, shear flow, steady-unsteady transition.

Effort sponsored by grants ARO W911NF-04-D-0004, AFOSR F49620-03-1-0098, NSF DMS-0308019, and NASA URETI NCC-1-02037.

various bifurcations of the 3-dimensional Doi model using spherical harmonic expansions and AUTO. Forest, Wang and Zhou [10, 11] provided the 3-dimensional Doi-Hess kinetic phase diagram, giving all attracting steady, periodic, and irregular orientational distributions versus shear rate and polymer concentration.

Amid all of these results, one of the classical issues of anisotropic molecular liquids, dating back to Onsager and de Gennes, is *what survives from orientational degeneracy of the quiescent nematic phase just as an external field perturbation is turned on.* This issue was bypassed in the continuum liquid crystal theory of Leslie and Ericksen, which did not involve an excluded-volume potential. The Leslie material parameters produced either a shear flow-aligning or a tumbling liquid crystalline fluid, with no freedom to transition between them, by varying experimental conditions such as volume fraction of the nematic polymer solvent mixture or the shear rate. Furthermore, there was no dynamics without an external field (hydrodynamic, electric or magnetic). For liquid crystalline polymers, however, the experimental evidence was mounting in the 1980's for not only an equilibrium 1^{st}-order isotropic-nematic phase transition, but a shear rate-dependent, steady-unsteady transition (Kiss & Porter '78, '80) which was accompanied by sign change in the first normal stress difference. The kinetic theory of Hess and Doi, and mesoscopic second-moment tensor approximations of Landau-de Gennes type (de Gennes & Prost '93, Beris & Edwards '95), became the focus of intense theoretical and numerical study to explain the shear behavior of nematic polymers. We refer the reader to several informative papers (Hinch & Leal '76, Marrucci & Greco '93, Larson & Öttinger '91, Burghardt '98, Berry & Tan '01, Rey & Denn '02, Forest & Wang '03, Kroger '04).

This paper addresses the question posed above for a model 2 dimensional liquid, physically motivated by monolayer films. Thin films of liquid crystalline polymers have been of considerable interest due to their stability and nonlinear optical properties compared to that of low molecular weight materials [20]. Maffetone *et al.* [20] showed the two-dimensional model proposed by Marrucci and Maffetone [22] could quantitatively predict the dynamic behavior of thin films under planar extensional flow. Maruyama *et al.* [21] examined the orientation dynamics of monolayer nematic polymer films for both extensional and simple shear flows. They obtained evidence of wagging (finite amplitude oscillations) and flow alignment in simple shear flow, depending on shear rate.

There is a *qualitative* difference between two-dimensional and three-dimensional isotropic-nematic transitions. In three dimensions, the transition is first order, discontinuous and the phase diagram exhibits hysteresis. On the other hand, mean field theory predicts that the transition should be second-order and continuous in two dimensions (cf. [22, 6, 11], Fig. 1, 2). The other important feature distinctions are "degree of degeneracy" of nematic phases, and the discrete number of ordered phases: In three dimensions, there are two types of ordered phases with distinct degrees of orientation and different "shapes" of the orientational distribution with one stable and the other unstable. The unstable branch does play a role in shear-dependent bifurcation diagrams as those branches subsequently collide with others [8]. In two dimensions, there is only one nematic phase; the "lower branch" is identical to the upper branch associated with a $\mathbb{Z}_2$-symmetry [12] unique to two-dimensional liquids, explained below. Thus, subsequent bifurcations in shear flows with other applied fields will be qualitatively distinct.

The purpose of this paper is to analytically solve the two-dimensional weak shear problem. That is, we aim to rigorously explain how the 2D quiescent phase diagram versus dimensionless concentration N extends in the two parameter space of (N, Pe), where Pe is the dimensionless shear rate, and to understand whether the extreme sensitivity to closure rule of 3-dimensional nematic liquids [8] also obtains in two-dimensional orientational dynamics.

2. **Kinetic theory and mesoscopic models.** Let $f(\mathbf{m}, t)$ be the orientational probability distribution function (PDF) that the axis of revolution of the molecule has an orientation given by the unit vector $\mathbf{m}$=$(\cos\theta, \sin\theta)$ at time t. The Doi-Hess theory gives an evolution equation for the PDF $f(\mathbf{m}, t)$,

$$\frac{\partial f}{\partial t} = D_r^0 \frac{\partial}{\partial \mathbf{m}} \cdot [\frac{\partial f}{\partial \mathbf{m}} + \frac{f}{k_B T} \frac{\partial V_{MS}}{\partial \mathbf{m}}] - \frac{\partial}{\partial \mathbf{m}} \cdot (\dot{\mathbf{m}} f), \tag{1}$$

where D_r^0 is an averaged rotary diffusivity or relaxation rate, k_B is the Boltzman constant, T is the absolute temperature. The first term in (1) is Brownian diffusion on the sphere. The second term is due to molecule interactions, explained further below. The third term is the flow coupling through the velocity gradient,

$$\nabla \mathbf{v} = \mathbf{\Omega} + \mathbf{D}, \tag{2}$$

where $\mathbf{\Omega}$ is the vorticity tensor and $\mathbf{D}$ is the rate of strain tensor given by

$$\mathbf{\Omega} = \frac{1}{2}(\nabla \mathbf{v} - \nabla \mathbf{v}^T), \ \mathbf{D} = \frac{1}{2}(\nabla \mathbf{v} + \nabla \mathbf{v}^T), \tag{3}$$

$$\dot{\mathbf{m}} = \mathbf{\Omega} \cdot \mathbf{m} + a[\mathbf{D} \cdot \mathbf{m} - \mathbf{D} : \mathbf{mmm}]. \tag{4}$$

This is the so-called Jeffery orbit for spheroids in Stokes flow in a viscous solvent, where $-1 \le a \le 1$ is the molecular shape parameter related to the molecular aspect ratio r by

$$a = \frac{r^2 - 1}{r^2 + 1}. \tag{5}$$

We assume two-dimensional simple shear flow $\mathbf{v} = \dot{\gamma}(y, 0)$, where $\dot{\gamma}$ is the shear rate, for which the rate of strain and vorticity tensors are

$$\begin{array}{rclcrcl} \mathbf{D} & = & \dot{\gamma}\tilde{\mathbf{D}}, & & \mathbf{\Omega} & = & \dot{\gamma}\tilde{\mathbf{\Omega}} \\ \tilde{\mathbf{D}} & = & \frac{1}{2}\begin{pmatrix} 0 & 1 \\ 1 & 0 \end{pmatrix}, & & \tilde{\mathbf{\Omega}} & = & \frac{1}{2}\begin{pmatrix} 0 & 1 \\ -1 & 0 \end{pmatrix}. \end{array} \tag{6}$$

In (1), V_{MS} is the Maier-Saupe excluded-volume potential with strength proportional to the dimensionless polymer concentration N,

$$V_{MS} = -2Nk_BT\mathbf{mm} :< \mathbf{mm} > . \tag{7}$$

The second moment $\mathbf{M}$ of the PDF $f(\mathbf{m}, t)$ is prominent in any connections of theory to experimental data:

$$\mathbf{M} =< \mathbf{mm} >= \int_0^\pi \mathbf{mm} f(\mathbf{m}, t) d\mathbf{m}. \tag{8}$$

The map between light scattering intensity I in the plane of $\mathbf{m}$ and the orientational distribution function f is [21]

$$I = \frac{2\pi h s}{\omega}, \tag{9}$$

where h is the monolayer thickness, ω is the wavelength of the incident light and s is the Hermans orientation parameter determined from $\mathbf{M}$, equation (15). The

mesoscopic orientation tensor $\mathbf{Q} = \mathbf{M} - \frac{1}{2}\mathbf{I}$ is the traceless part of $\mathbf{M}$. Similarly, one represents higher moments of f with this bracket notation.

The nematodynamical equation for $\mathbf{Q}$ is derived from (1):

$$\begin{aligned}\frac{d}{dt}\mathbf{Q} &= \mathbf{\Omega}\cdot\mathbf{Q} - \mathbf{Q}\cdot\mathbf{\Omega} + a[\mathbf{D}\cdot\mathbf{Q} + \mathbf{Q}\cdot\mathbf{D}] + a\mathbf{D} - 2a\mathbf{D} :< \mathbf{mmmm} > \\ &\quad -6\mathbf{D}_r^0[\mathbf{Q} - N(\mathbf{Q} + \tfrac{1}{2}\mathbf{I})\cdot\mathbf{Q} + N\mathbf{Q} :< \mathbf{mmmm} >]. \end{aligned} \tag{10}$$

The variable coefficients in the linear Smoluchowski equation (1) translate to nonlinearity and coupling between moments in the moment equations, so that any finite moment truncation requires some closure approximation. Following tradition in polymeric systems, and motivated by a closed theory for the physically measurable second moment properties, many models have posited a closed equation for $\mathbf{M}$, respectively $\mathbf{Q}$. The Doi closure rule assumes $(\bullet) :< \mathbf{mmmm} >= (\bullet) :< \mathbf{mm} >< \mathbf{mm} >$; other closures due to Tsuji-Rey and Hinch-Leal are discussed and analyzed below.

We now non-dimensionalize the flow field and orientation dynamics (10) using the nematic relaxation time scale $(D_r^0)^{-1}$. The key dimensionless parameters are then the Peclet number $Pe = \frac{\dot{\gamma}}{D_r^0}$, the shear rate normalized relative to nematic relaxation rate, and the dimensionless concentration N. Hereafter, we work in dimensionless time $\tilde{t} = tD_r^0$.

3. Q-tensor representations.

3.1. **Component representation.** A component representation is a standard matrix representation with respect to a chosen coordinate system. The typical Cartesian representation of $\mathbf{Q}$ satisfies a symmetry constraint $Q_{xy} = Q_{yx}$ and a trace zero constraint $Q_{xx} + Q_{yy} = 0$ having two independent degrees of freedom. The symmetric traceless matrices form a two-dimensional vector space with standard basis

$$\mathbf{Q}^{(1)} = \begin{pmatrix} 1 & 0 \\ 0 & -1 \end{pmatrix}, \quad \mathbf{Q}^{(2)} = \begin{pmatrix} 0 & 1 \\ 1 & 0 \end{pmatrix}, \tag{11}$$

which have eigenvector frames $\{(1,0),(0,1)\}$ and $\{(1,1),(1,-1)\}$, respectively corresponding to eigenvalues 1 and -1. In this basis, the two independent components Q_{xx}, Q_{xy} are evident:

$$\mathbf{Q} = Q_{xx}\mathbf{Q}^{(1)} + Q_{xy}\mathbf{Q}^{(2)}. \tag{12}$$

For the Doi closure, the nematodynamic model (10) takes the following form using the component representation (12):

$$\begin{aligned} \dot{Q_{xx}} &= -6Q_{xx}(1 - \tfrac{N}{2} + 2N(Q_{xx}^2 + Q_{xy}^2)) + Pe(Q_{xy} - 2aQ_{xx}Q_{xy}) \\ \dot{Q_{xy}} &= -6Q_{xy}(1 - \tfrac{N}{2} + 2N(Q_{xx}^2 + Q_{xy}^2)) + Pe(-Q_{xx} + \tfrac{a}{2} - 2aQ_{xy}^2). \end{aligned} \tag{13}$$

3.2. **Spectral representation.** Since $\mathbf{Q}$ is symmetric, the eigenvectors of $\mathbf{Q}$ form an orthonormal basis of $\mathbb{R}^2$. From the spectral theorem, if d_i is the eigenvalue associated with eigenvector $\mathbf{n}_i$, then

$$\mathbf{Q} = \sum (d_i - \frac{1}{2})\mathbf{n}_i\mathbf{n}_i, \quad d_1 + d_2 = 1, \sum \mathbf{n}_i\mathbf{n}_i = \mathbf{I}. \tag{14}$$

It follows that $\mathbf{Q}$ has the spectral representation

$$\mathbf{Q} = s(\mathbf{n}_1\mathbf{n}_1 - \frac{\mathbf{I}}{2}), \ s = d_1 - d_2 = 2d_1 - 1, \tag{15}$$

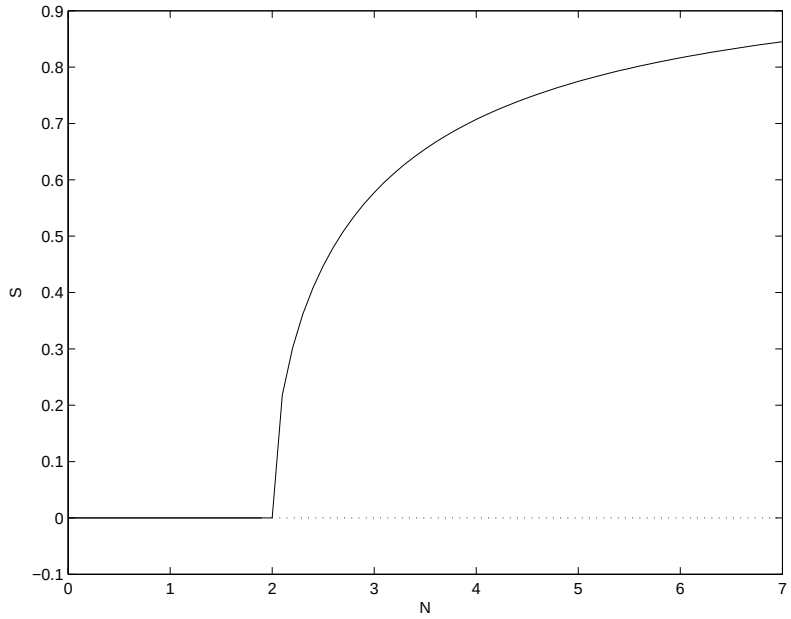

FIGURE 1. Isotropic-nematic transition diagram without flow of the 2D Doi closure model. The order parameter S is plotted against dimensionless concentration N. The stable isotropic solution becomes unstable and the stable nematic branch is born at $N = 2$. Solid (dashed) curves denote stable (unstable) equilibria.

where $\frac{1}{2}s$ is an eigenvalue of $\mathbf{Q}$ associated with major director $\mathbf{n} = (\cos\theta, \sin\theta)$.

The map between (Q_{xx}, Q_{xy}) and (s, θ) is

$$\begin{array}{rcl} Q_{xx} & = & \frac{s}{2}\cos 2\theta \\ Q_{xy} & = & \frac{s}{2}\sin 2\theta, \end{array} \tag{16}$$

and the Doi closure model (13) has an equivalent form:

$$\begin{array}{rcl} \dot{\theta} & = & -\frac{Pe}{2}(1 - \frac{a}{s}\cos 2\theta) \\ \dot{s} & = & -3(N(s^2-1)+2)s + aPe(1-s^2)\sin 2\theta. \end{array} \tag{17}$$

From (17), the quiescent 2D nematic liquid ($Pe \equiv 0$) has equilibria $s = 0$ (the isotropic state $\mathbf{Q} = \mathbf{0}$) for all N, and nematic equilibria

$$s_\pm = \pm\sqrt{1 - \frac{2}{N}}, \tag{18}$$

for $N > 2$. From the first equation of (17), the director for nematic equilibria is arbitrary, which is known as orientational degeneracy. From the second equation of (17), one easily finds $s = 0$ is stable for $N < 2$ and unstable for $N \geq 2$, whereas $s_\pm$ are stable in the order parameter direction, while neutral in the θ direction. This explains Fig. 1.

In any closure model, (17) takes the form $\dot{\theta} = -\frac{Pe}{2}(1 - \lambda_L \cos 2\theta)$, where λ_L is the 2-dimensional analog of the Leslie alignment parameter. This parameter gives an explicit criterion for steady equilibria ($|\lambda_L| > 1$) versus unsteady behavior

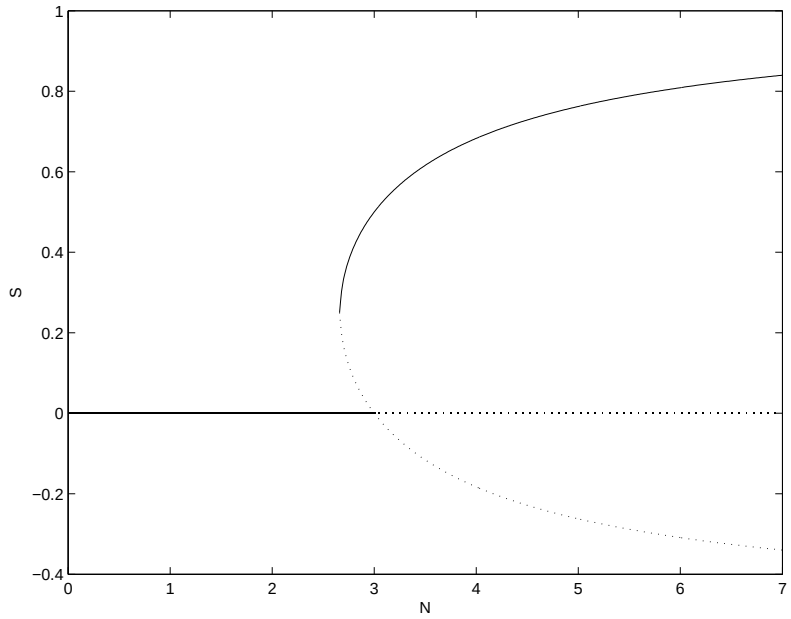

FIGURE 2. Isotropic-nematic transition diagram for 3D nematic liquids. The equilibrium branches $s_0 = 0$ and $s_\pm = \frac{1\pm 3\sqrt{1-\frac{8}{3N}}}{4}$ are given for the Doi closure model with solid (dotted) curves representing stable (unstable) equilibria.

($|\lambda_L| < 1$), and also encodes the closure rule. For the Doi closure, $\lambda_L = \frac{a}{s}$; for other closures, the form is given in Appendix B.

We now make note of a discrete symmetry that is special to two dimensions, which has consequences for the isotropic-nematic phase diagram as shown in Fig. 1. From (14), $\mathbf{Q}$ can be represented by either $s_+, \mathbf{n}_1$ or $s_-, \mathbf{n}_2$, and the representations are identical:

$$\mathbf{Q} \;=\; s_+\Big(\mathbf{n}_1\mathbf{n}_1 - \frac{1}{2}\mathbf{I}\Big) = -s_+\Big(\mathbf{n}_2\mathbf{n}_2 - \frac{1}{2}\mathbf{I}\Big) = s_-\Big(\mathbf{n}_2\mathbf{n}_2 - \frac{1}{2}\mathbf{I}\Big). \tag{19}$$

This implies, in stark contrast to the 3-dimensional nematic equilibrium sets, that there is only one nematic branch, i.e. the s_--branch is identical to the s_+-branch, thus the terminology $\mathbb{Z}_2$-symmetry [12]. This observation has significant physical consequences, captured in the bifurcation structure associated with simultaneous instability of the isotropic branch and onset of the nematic branch. This bifurcation is depicted in Fig. 1 and is called a pitchfork bifurcation with $\mathbb{Z}_2$-symmetry. By comparison with Fig. 2 for 3-dimensional molecular liquids, the dotted lower branch of unstable "oblate" nematic phases does not exist in 2D. Thus, the only orientation state for which the major director is not unique (the definition of a defect) is the isotropic state, $\mathbf{Q} = \mathbf{0}$. In 3D, there are additional phases where the major director lies on a circle, giving another class of defects.

4. **Weak-shear solvability conditions for persistence of equilibria.** We now follow [10] to assess persistence of the isotropic and S^1-invariant branches of solutions in Fig. 1 in the presence of a weak shear flow. This is accomplished by

parametrizing all equilibria of (18) and then deriving solvability conditions at next order in the weak flow parameter Pe.

Assume weak shear, $Pe \ll 1$, and expand $\mathbf{Q}$ in powers of Pe:

$$\mathbf{Q} = \mathbf{Q}_0 + Pe\mathbf{Q}_1 + Pe^2\mathbf{Q}_2 + \cdots . \tag{20}$$

We seek those equilibria $\mathbf{Q}_0$ which survive in weak shear and $\mathbf{Q}_1$ is the leading shear-dependent correction. At order Pe, for any mesoscopic tensor model (10), $\mathbf{Q}_1$ must satisfy a linearized tensor-operator equation,

$$\mathbf{A}_1(\mathbf{Q}_0)\cdot\mathbf{Q}_1 = \mathbf{r}_1(\mathbf{Q}_0), \tag{21}$$

where $\mathbf{A}_1(\mathbf{Q}_0)$ corresponds to rotational diffusion and linearized Maier-Saupe potential, and $\mathbf{r}_1(\mathbf{Q}_0)$ is the linearized flow perturbation. With the Doi closure model, these operators are given by

$$\begin{aligned} \mathbf{A}_1(\mathbf{Q}_0)\cdot\mathbf{Q}_1 &= 6[\mathbf{Q}_1 - N(\mathbf{M}_0\cdot\mathbf{Q}_1 + \mathbf{Q}_1\cdot\mathbf{Q}_0) \\ &\quad +N((\mathbf{Q}_0:\mathbf{M}_0)\mathbf{Q}_1 + (\mathbf{Q}_0:\mathbf{Q}_1)\mathbf{M}_0 + (\mathbf{Q}_1:\mathbf{M}_0)\mathbf{M}_0)], \\ \mathbf{r}_1(\mathbf{Q}_0) &= \tilde{\mathbf{\Omega}}\cdot\mathbf{Q}_0 - \mathbf{Q}_0\cdot\tilde{\mathbf{\Omega}} + a[\tilde{\mathbf{D}}\cdot\mathbf{Q}_0 + \mathbf{Q}_0\cdot\tilde{\mathbf{D}}] \\ &\quad +a\tilde{\mathbf{D}} - 2a\tilde{\mathbf{D}}:\mathbf{M}_0\mathbf{M}_0 \end{aligned} \tag{22}$$

where $\mathbf{M}_0 = \mathbf{Q}_0 + \frac{1}{2}\mathbf{I}$. The Fredholm alternative theorem yields the weak-shear solvability condition [16, 10]:

$$\mathbf{r}_1(\mathbf{Q}_0) \perp \mathcal{N}[\mathbf{A}_1^T(\mathbf{Q}_0)], \tag{23}$$

where $\mathcal{N}$ denotes the null space of the matrix $\mathbf{A}_1^T$. This solvability condition must be satisfied by these quiescent states $\mathbf{Q}_0$ in (18) which persist as steady states in weak shear, arising either from the stable nematic equilibrium or isotropic equilibria.

4.1. **The shear-perturbed, nearly isotropic branch.** The isotropic steady state perturbs at $O(Pe)$ to a unique, explicit branch of equilibria,

$$\mathbf{Q} = \mathbf{0} + Pe\frac{a}{3(2-N)}\tilde{\mathbf{D}} + O(Pe^2), \tag{24}$$

where $\tilde{\mathbf{D}}$ is the normalized rate-of-strain for pure shear. The directors of $\mathbf{Q}$ are

$$\mathbf{n}_1 = (1,1), \quad \mathbf{n}_2 = (1,-1), \tag{25}$$

with corresponding distinct order parameters

$$d_1 = \frac{1}{2} + \frac{a}{6(2-N)}Pe, \quad d_2 = \frac{1}{2} - \frac{a}{6(2-N)}Pe. \tag{26}$$

Note that the Leslie alignment angle $\theta \equiv \frac{\pi}{4}$ from $\mathbf{n}_1 = (1,1) = (\cos\theta, \sin\theta)$, at leading order in Pe for all concentrations away from $N = 2$. This is consistent with 3D kinetic [11] and mesoscopic [10] analysis. The degree of anisotropy is measured by $|d_1 - d_2|$, and for $|N-2| > Pe$, the Flory order parameter $|d_1 - d_2|$ is proportional to the presumed weak normalized shear rate, Pe.

The next order solvability condition,

$$\mathbf{A}_2(\mathbf{Q}_0, \mathbf{Q}_1)\cdot\mathbf{Q}_2 = \mathbf{r}_2(\mathbf{Q}_0, \mathbf{Q}_1), \tag{27}$$

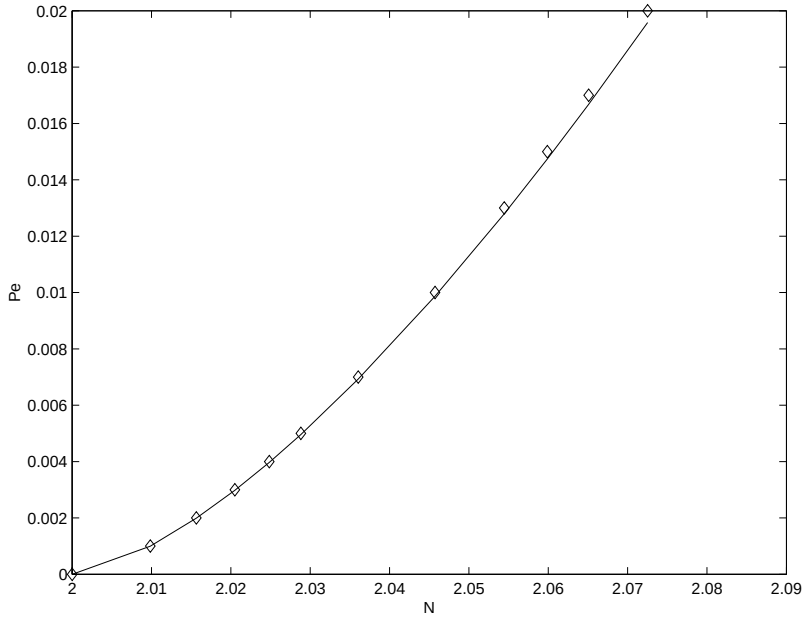

FIGURE 3. The scaling behavior of the bifurcation point LP2, Fig. 5. The solid line is the analytical prediction, while the diamonds represent LP2 points obtained by AUTO. These bifurcation points represent the locus of turning points where the unstable isotropic branch and the unstable nematic branch are connected.

determines stability of the persistent equilibria (24). For the Doi closure model, the operators in (27) are given by

$$\begin{aligned}\mathbf{A}_2(\mathbf{Q}_0,\mathbf{Q}_1)\cdot\mathbf{Q}_2 &= 6[\mathbf{Q}_2 - N(\mathbf{M}_0\cdot\mathbf{Q}_2+\mathbf{Q}_2\cdot\mathbf{Q}_0)\\ &\quad +N(\mathbf{Q}_0:\mathbf{M}_0\mathbf{Q}_2+(\mathbf{Q}_2:\mathbf{M}_0+\mathbf{Q}_0:\mathbf{Q}_2)\mathbf{M}_0)],\\ \mathbf{r}_2(\mathbf{Q}_0,\mathbf{Q}_1) &= \tilde{\mathbf{\Omega}}\cdot\mathbf{Q}_1-\mathbf{Q}_1\cdot\tilde{\mathbf{\Omega}}+a[\tilde{\mathbf{D}}\cdot\mathbf{Q}_1+\mathbf{Q}_1\cdot\tilde{\mathbf{D}}]\\ &\quad -2a(\tilde{\mathbf{D}}:\mathbf{M}_0\mathbf{Q}_1+\tilde{\mathbf{D}}:\mathbf{Q}_1\mathbf{M}_0)\\ &\quad +6[N\mathbf{Q}_1\cdot\mathbf{Q}_1-N((\mathbf{Q}_1:\mathbf{M}_0+\mathbf{Q}_0:\mathbf{Q}_1)\mathbf{Q}_1+\mathbf{Q}_1:\mathbf{Q}_1\mathbf{M}_0)].\end{aligned} \tag{28}$$

The operator $-\mathbf{A}_2$ has explicit linearized eigenvalues,

$$\lambda_1 \approx \lambda_2 = -3(2-N)+O(Pe), \tag{29}$$

from which we deduce the shear-perturbed isotropic branch is stable for $N<2$ and unstable for $N>2$. These results give detailed information about the corresponding solution branches with $|Q_{xx}| \ll 1$ in Fig. 4 (Leslie angles) and Fig. 5, where solid (dotted) lines indicate stable (unstable) states. The transition region surrounding $N=2$ is treated next.

4.2. **Persistence of the I-N transition, i.e. the $\mathbb{Z}_2$-symmetric pitchfork bifurcation.** Near $N=2$, the expansion (24) breaks down. This suggests we need a different scaling in (20), e.g. a Pe^α expansion in a neighborhood of the isotropic-nematic transition $N=2$ for small Pe. See, Doi and Larson [25] calculated this scaling, $Pe^{\frac{1}{2}}$, in the 3-dimensional case, which was confirmed by Forest, Wang and Zhou [11] in their analysis of all solution branches.

To capture the scaling behavior for persistence of the $\mathbb{Z}_2$-symmetric pitchfork bifurcation at $N = 2$, in Fig. 1, we impose two solvability conditions from (13). First, persistence of equilibria will yield 2 scalar equations, then a neutral (or marginal) stability condition on these equilibria yields a third condition. Together, these criteria give 3 conditions in (Q_{xx}, Q_{xy}, N, Pe), whose 1-parameter family of solutions gives the curve of persistent bifurcation values (N, Pe), together with the $\mathbf{Q}$-tensor along the curve. For the Doi closure, the equilibria at leading order in Pe satisfy

$$H_1 = -6Q_{xx}(1 - \frac{N}{2} + 2N(Q_{xx}^2 + Q_{xy}^2)) = 0 \tag{30}$$

$$H_2 = -6Q_{xy}(1 - \frac{N}{2} + 2N(Q_{xx}^2 + Q_{xy}^2)) + Pe\frac{a}{2} = 0. \tag{31}$$

The marginal stability condition [25] is

$$DET\frac{\partial(H_1, H_2)}{\partial(Q_{xx}, Q_{xy})} = 0. \tag{32}$$

This yields

$$72NQ_{xx}Q_{xy}[2 + N(-1 + 4Q_{xx}^2 - 8Q_{xx}Q_{xy} + 12Q_{xy}^2)] = 0. \tag{33}$$

Solving these three equations in a neighborhood of $N = 2$, $Pe = 0$, we obtain the 2D scaling behavior

$$Pe \simeq \frac{2}{a\sqrt{3}}[\frac{(N-2)^3}{N}]^{1/2}. \tag{34}$$

This behavior is quite different from the analogous 3D result [25, 11]. In Fig. 3, this 2D scaling prediction is compared with eleven (11) bifurcation diagrams for fixed finite values $0 < Pe < 0.02$, employing the continuation software AUTO. One such representative bifurcation diagram is given in Fig. 5 for $Pe = 0.1$; the data point labeled LP2 is the object of the formula (34) and provides one data point in Fig. 3.

4.3. **The nematic equilibrium branch.** We parameterize the S^1 invariant director $\mathbf{m}_0$ by $\mathbf{m}_0 = (\cos\theta, \sin\theta)$. As explained earlier, the unique nematic equilibrium branch has order parameter $s_+ = \sqrt{1 - \frac{2}{N}}$. Therefore the nematic equilibrium has an explicit representation:

$$\mathbf{Q}_0 = s_+(\mathbf{m}_0\mathbf{m}_0 - \frac{\mathbf{I}}{2}) = \frac{s_+}{2}\begin{pmatrix} \cos 2\theta & \sin 2\theta \\ \sin 2\theta & -\cos 2\theta \end{pmatrix}. \tag{35}$$

The solvability equation (21) has the following ingredients for the nematic phase:

$$\mathbf{A}_1 = \frac{6s_+^2}{1 - s_+^2}\begin{pmatrix} 1 + \cos 4\theta & \sin 4\theta \\ \sin 4\theta & 2\sin^2 2\theta \end{pmatrix}, \tag{36}$$

$$\mathbf{r}_1 = \begin{pmatrix} \frac{1}{2}s_+(1 - as_+\cos 2\theta)\sin 2\theta, \\ -\frac{1}{2}s_+\cos 2\theta + \frac{a}{4}(2 - s_+^2(1 - \cos 4\theta)) \end{pmatrix}. \tag{37}$$

The eigenvalues of the system are:

$$-\frac{Pe}{2}(4 - 4s_+^2 + 3as_+\cos 2\theta)\tan 2\theta, \quad -\frac{12s_+^2}{1 - s_+^2} + O(Pe) \tag{38}$$

with corresponding vectors

$$v_1 = (-\tan 2\theta, 1), \; v_2 = (\cot 2\theta, 1). \tag{39}$$

If $N > 2$, the eigenvector v_1 spans the null space of $\mathbf{A}_1^T$, so the solvability condition

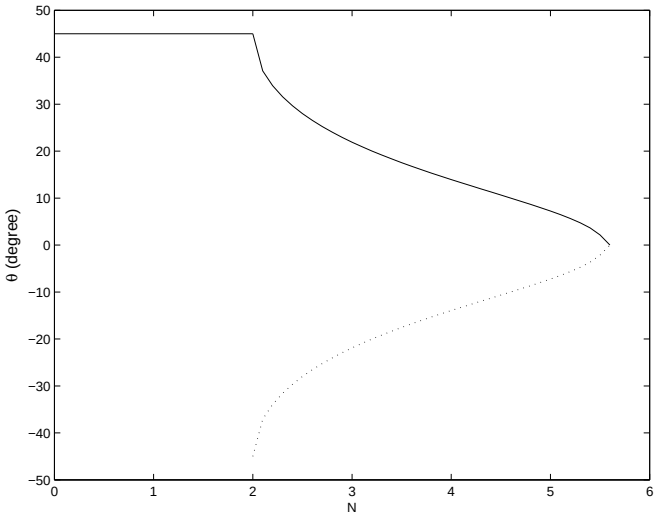

FIGURE 4. The steady state Leslie alignment angle θ, formula (40), plotted versus nematic concentration N for aspect ratio $r = 3$. The solid (dotted) lines represent stable (unstable) solutions.

simplifies to $\mathbf{r}_1^T v_1 = 0$. After simplification, we get $\mathbf{r}_1^T v_1 = \frac{1}{2}(a - s\sec 2\theta)$, which produces the Leslie alignment angle in weak shear for the Doi closure

$$\cos 2\theta = \frac{s_+}{a} = \frac{1}{a}\sqrt{1 - \frac{2}{N}} \equiv 1/\lambda_L, \tag{40}$$

where λ_L is the Leslie alignment parameter mentioned in Section 3. For $|\lambda_L| < 1$, any solution that exists must be unsteady. If $|\lambda_L| > 1$, the equation (40) has two distinct steady solutions (one stable and one unstable),

$$\theta = \frac{1}{2}\arccos\frac{s_+}{a}, \tag{41}$$

for $-\frac{\pi}{2} < \theta < \frac{\pi}{2}$. From (38) and (40), the solution is stable if $-\frac{\pi}{2} < \theta < -\frac{\pi}{4}$ when a is negative (i.e. disk-like molecules) or $0 < \theta < \frac{\pi}{4}$ when a is positive (i.e. rod-like molecules). Otherwise, the solution is unstable. This yields agreement with Fig. 5 predicting the upper two (solid and dotted) curves between LP1 and LP2.

We solve the linear system (21) as well as the next order system (27), which yields:

$$\mathbf{Q} = \mathbf{Q}_0 + Pe\frac{(1 - s_+^2)^2}{12 s_+}\begin{pmatrix} 2\sin 2\theta & -\cos 4\theta \sec 2\theta \\ -\cos 4\theta \sec 2\theta & -2\sin 2\theta \end{pmatrix} + O(Pe^2). \tag{42}$$

- For infinite aspect ratio $|a| = 1$, the right hand side of (40) always has modulus less than 1, i.e. $\mathbf{Q}_1$ is solvable.
- For $|a| < 1$, the right hand side of (40) will hit values ± 1 at a critical concentration N. The relationship between this critical concentration and the aspect ratio r is discovered as

$$N_*(a) = \frac{2}{1 - a^2} = \frac{1}{2}\left(r + \frac{1}{r}\right)^2. \tag{43}$$

  – For $2 < N \le N_*(a)$, $\mathbf{Q}_1$ is solvable, i.e. steady solutions exist.

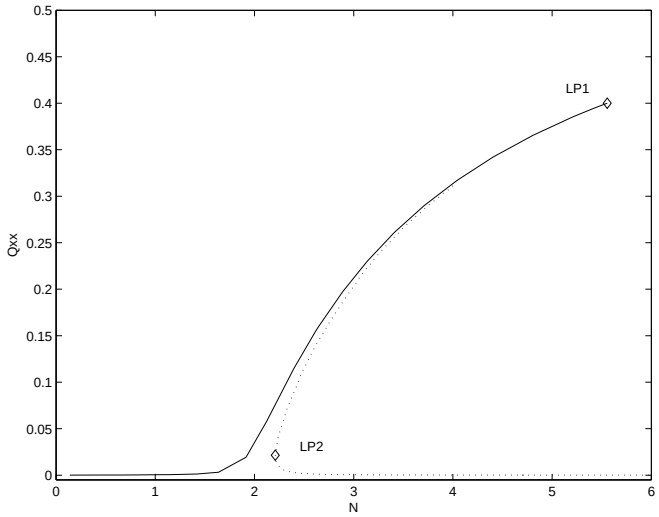

FIGURE 5. Steady state solution branches of the Doi closure model are plotted for $Pe = 0.1$ using AUTO. Two folds exist at N=2.21 and 5.556. The unsteady regime starts at N=5.556.

– For $N > N_*(a)$, no steady solution exists for $\mathbf{Q}_1$.

$N_*(a)$ predicts the AUTO generated bifurcation LP1, which represents the termination of a steady state solution branch. For $r = 3$ or $r = 1/3$, $N_*(a) = N_*(\pm 0.8) \approx 5.556$, which yields the point LP1 in Fig. 5. Marrucci and Maffettone [22] predicted $N_*(a) = 2.41$ for the rigid rod ($a = 1$) kinetic model, but the meaning of parameters N and a is blurred in the projection onto second moment models.

5. **Limit cycles in unsteady regimes.** The next task is to characterize oscillatory solutions at the onset of simple shear, beyond the statement that they are expected since $|\lambda_L(a, N)| < 1$ in formula (40).

Theorem 5.1. *For sufficiently small $Pe \neq 0$ and $N > N_*(a) = \dfrac{2}{1-a^2}$, there exists a stable limit cycle of* (13)*, equivalently* (17).

Proof. The Poincaré-Bendixson Theorem states that in a closed, bounded subset R of the plane, if R has no fixed points and there exists a trajectory C that is confined in R, then R contains a closed orbit, i.e. a limit cycle. To be sure that a confined trajectory C exists, we will show there is a trapping region R, i.e. a closed connected set such that the vector field points inward everywhere on the boundary of R.

If $N > \dfrac{2}{1-a^2}$, then the Leslie parameter λ_L obeys $|\lambda_L| < 1$. From (17), $\dot{\theta}$ can never be zero. Thus there is no fixed point. Since $-1 \leq a(1-s^2)\sin 2\theta \leq 1$,

$$-3s[N(s^2-1)+2] - Pe \leq \dot{s} \leq -3s[N(s^2-1)+2] + Pe.$$

For sufficiently small Pe, we can assume $\dot{s} \approx -3s[N(s^2-1)+2]$. If we choose $s_{max}^2 = 1 + \varepsilon_1 - \dfrac{2}{N}$, where $0 < \varepsilon_1 < \frac{2}{N}$, then $\dot{s}_{max} \approx -3s_{max}(\varepsilon_1 N) < 0$. If we choose $s_{min}^2 = 1 - \varepsilon_2 - \dfrac{2}{N}$, where $0 < \varepsilon_2 < 1 - \frac{2}{N}$, then $\dot{s}_{min} \approx 3s_{min}(\varepsilon_2 N) > 0$.

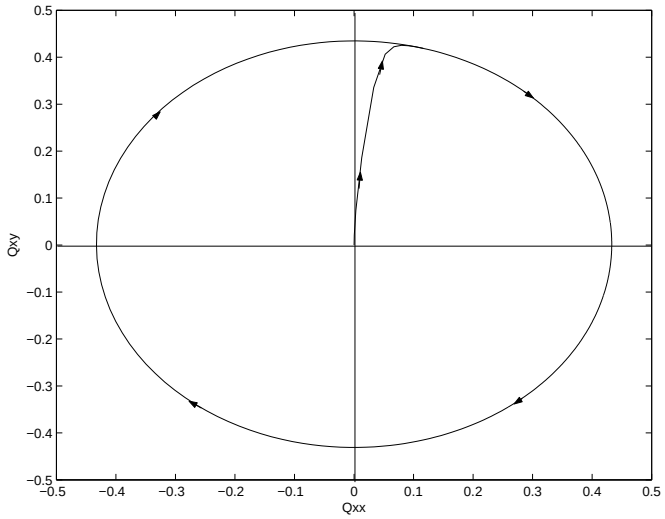

FIGURE 6. Convergence of a sample orbit to the tumbling limit cycle for N=8, Pe=0.66, a=0.8, in the Doi closure model.

Hence by the Poincaré-Bendixson Theorem, there exists a closed orbit. □

To characterize the bifurcation N_* following [27], we expand the equation (17) using the method of two time scales as $Pe \to 0$; the fast $O(1)$ time scale $T_0 = t$ and slow time scale $T_1 = Pe \cdot t$. Then the expansions are

$$s = s_0(T_0, T_1) + Pe \cdot s_1(T_0, T_1) + O(Pe^2) \tag{44}$$

$$\theta = \theta_0(T_0, T_1) + Pe \cdot \theta_1(T_0, T_1) + O(Pe^2). \tag{45}$$

At leading order, the equations give $s_0 = s_+ = \sqrt{1 - \frac{2}{N}}$, $\partial\theta_0/\partial T_0 = 0$ and so $\theta_0(T_0, T_1) = \Theta_0(T_1)$. At first order in Pe,

$$\theta_1 = -T_0[\frac{d\Theta_0}{dT_1} + \frac{1}{2}(1 - \frac{a}{s_0}\cos 2\Theta_0)] + C(T_1), \tag{46}$$

where $C(T_1)$ is a function of T_1 alone. To make θ_1 independent of T_0,

$$\frac{d\Theta_0}{dT_1} + \frac{1}{2}(1 - \frac{a}{s_0}\cos 2\Theta_0) = 0. \tag{47}$$

So, the period of the periodic orbit is

$$T = \frac{4\pi s_0}{Pe\sqrt{s_0^2 - a^2}}. \tag{48}$$

This shows that the period of the limit cycle is infinite as s_0 goes to a. Since $s_0 = \sqrt{1 - \frac{2}{N}}$ for $Pe \ll 1$, the period goes to infinity as $N \to N_*(a) = \frac{2}{1-a^2}$, as confirmed by AUTO in Fig. 7 by passing from Region 4 into Region 2.

6. **The phase diagram of mesoscopic models: Robustness vs sensitivity to closure.** In this section we summarize the behavior of a liquid crystal polymer monolayer in shear flow in terms of phase diagrams. We calculate steady state

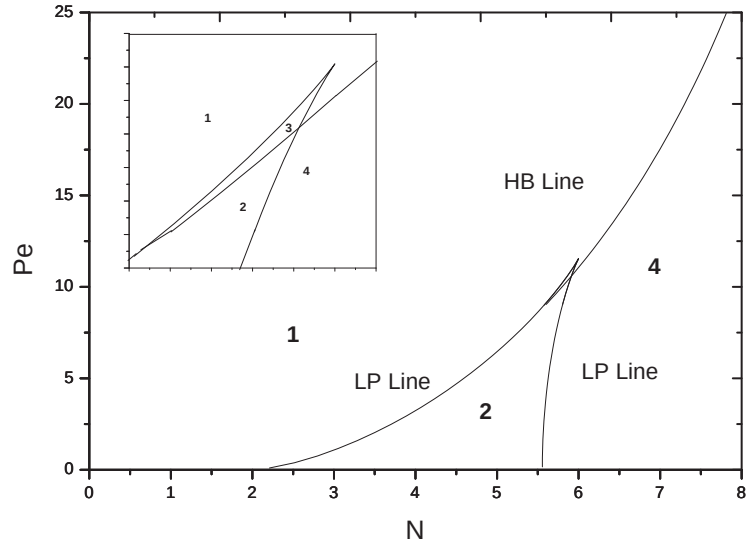

FIGURE 7. N-Pe phase diagram of the 2D Doi closure model. The parameter space is divided into 4 regions. The Regions 1, 2, 3 are governed by flow-aligning states whereas Region 4 has tumbling or wagging, stable limit cycles.

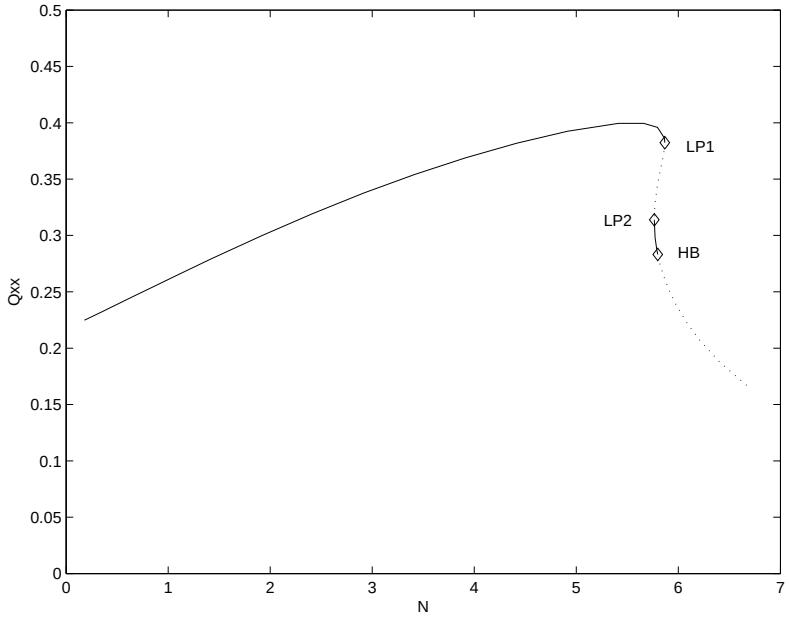

FIGURE 8. The steady state solutions of the Doi closure model for $Pe = 10$.

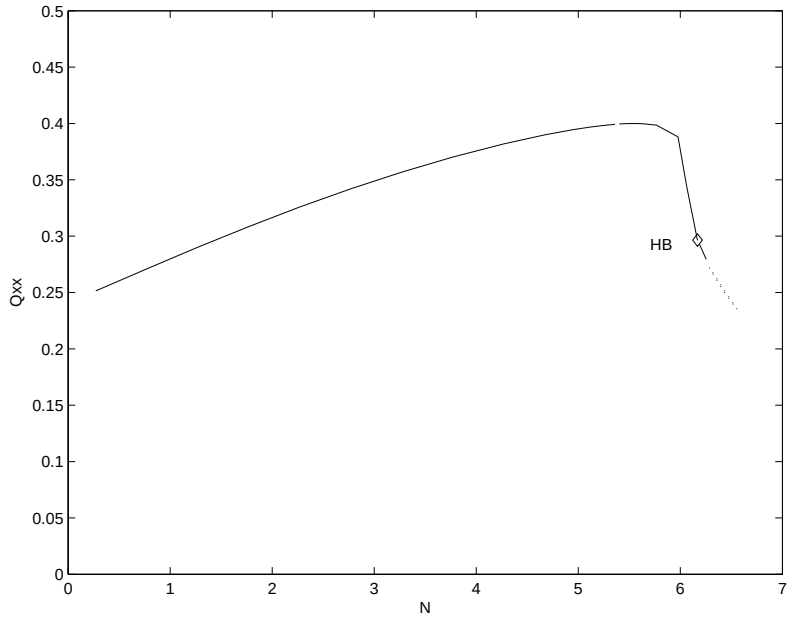

FIGURE 9. The steady state solution of the Doi closre model for $Pe = 12$.

solutions and bifurcation branches, using XPPAUT and AUTO 97 for several closure models. The aspect ratio parameter is fixed as $a = 0.8$ in each model.

Fig. 7 is the phase diagram for the Doi closure in (N, Pe)-space. This figure shows that Hopf bifurcation ends at a limit point LP2. Vicente Alonso showed this point is a so-called Bogdanov-Takens bifurcation in a 3D Landau-de Gennes model [27]. The parameter space is separated into 4 regions:

Region 1: There is only one stable steady state solution, the perturbed isotropic phase.

Region 2: There are one stable and two unstable states (Fig. 5).

Region 3: There are two stable steady states. The nematic steady state is destabilized by the Hopf bifurcation (Fig. 8).

Region 4: There is one unstable steady state and a stable limit cycle. The limit cycle is generated by a global bifurcation called a saddle homoclinic bifurcation until $O(Pe) \sim 1$. For larger values of Pe, the limit cycle emanates from a Hopf bifurcation (Fig. 9).

The bifurcation diagram for the Doi model and that of the Hinch-Leal 1 model, Fig. 10, are able to capture the Bogdanov-Takens bifurcation [27] which is faithful to the 2D kinetic phase diagram [19]. Fig. 10 and Fig. 11 show the Hinch-Leal and Tsuji-Rey closures compress Region 3 so that detection of this aspect of the dynamical system is extremely sensitive to numerical error.

7. **Conclusion.** In this paper, we derived weak-shear steady and unsteady selection criteria for two-dimensional nematic polymers using various second-moment closures. These results are valid except in a neighborhood of the isotropic-nematic transition at $N = 2$; the persistence of this bifurcation point for low Pe is deduced by methods similar to See *et al.* [25] and Forest *et al.* [11] for three-dimensional

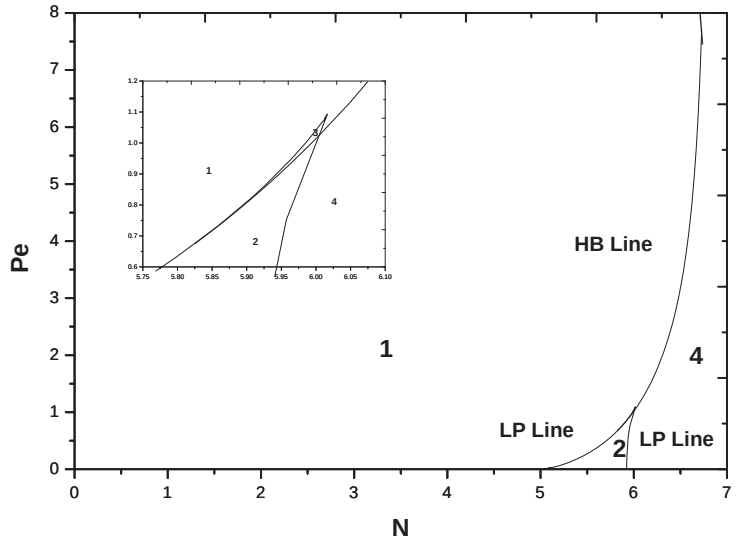

FIGURE 10. N-Pe Phase diagram for the Hinch-Leal 1 model. The 4 regions are same as the Doi model.

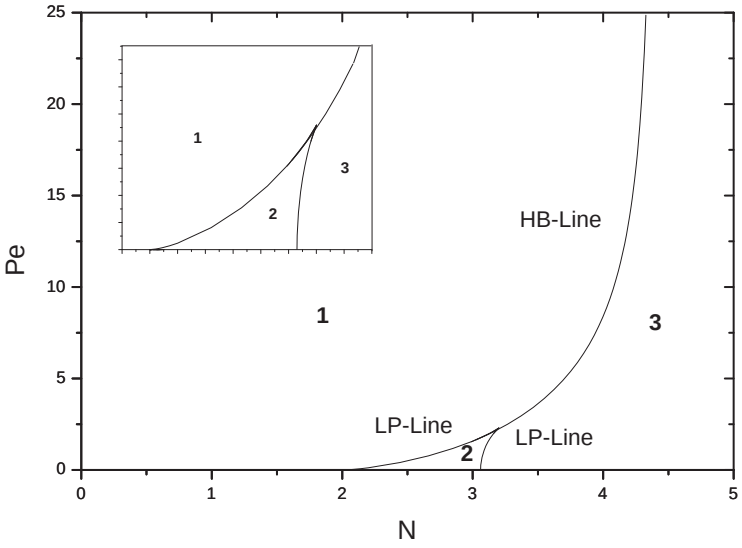

FIGURE 11. N-Pe Phase diagram of the Tsuji-Rey model. The aspect parameter ratio a is fixed at 0.8. Regions 1,2 consist of flow-aligning states while Region 3 has tumbling-wagging limit cycles.

nematic liquids. The analysis is then confirmed with numerical simulations using the continuation software AUTO. We showed the existence of a limit cycle beyond the parameter boundary for the steady-unsteady transition as an application of the Poincaré-Bendixon Theorem and characterized the transition boundary in the phase diagram in the weak shear limit. The shear-perturbed 2D phase diagrams for the three closure models (Doi, Tsuji-Rey and Hinch-Leal 1) are remarkably robust relative to the 3D shear problem.

Appendix A. **Closure approximations for 2D models.**
∘ Quadratic (Doi) Closure

$$(\bullet) :< \mathbf{mmmm} > \quad = \quad (\bullet) : \mathbf{MM}. \tag{49}$$

∘ Tsuji-Rey (TR) Closure

$$\begin{aligned} (\bullet) :< \mathbf{mmmm} > \quad = \quad & \tfrac{1}{4}[((\bullet) : \mathbf{Q})\mathbf{Q} + (\bullet) \cdot \mathbf{Q}^2 + \mathbf{Q} \cdot (\bullet) \cdot \mathbf{Q} + \mathbf{Q}^2 \cdot (\bullet) \\ & -(((\bullet) \cdot \mathbf{Q}) : \mathbf{Q})\mathbf{I}] + \tfrac{1}{2}((\bullet) : \mathbf{Q})\mathbf{I}. \end{aligned} \tag{50}$$

∘ Hinch-Leal 1 (HL1) Closure

$$\begin{aligned} (\bullet) :< \mathbf{mmmm} > \quad = \quad & \tfrac{1}{5}[6\mathbf{M} \cdot (\bullet) \cdot \mathbf{M} - (\mathbf{MM}) : (\bullet) \\ & -2((\mathbf{MM}) : (\bullet) - \mathbf{M} : (\bullet))\mathbf{I}]. \end{aligned} \tag{51}$$

∘ Hinch-Leal 2 (HL2) Closure

$$\begin{aligned} (\bullet) :< \mathbf{mmmm} > \quad = \quad & \mathbf{M}(\mathbf{M} : (\bullet)) \\ & +2[\mathbf{M} \cdot (\bullet) \cdot \mathbf{M} - \mathbf{M}^2(\mathbf{M}^2 : (\bullet))/(\mathbf{I} : \mathbf{M}^2)] \\ & +\alpha(\mathbf{M})[\tfrac{52}{315}(\bullet) - \tfrac{8}{21}[(\bullet) \cdot \mathbf{M} + \mathbf{M} \cdot (\bullet) - (\mathbf{M} : (\bullet))\mathbf{I}]] \end{aligned} \tag{52}$$

where

$$\alpha(\mathbf{M}) = \exp[2(\mathbf{I} - 3\mathbf{M}^2 : \mathbf{I})/(\mathbf{I} - \mathbf{M}^2 : (\bullet))\mathbf{I}]]. \tag{53}$$

Appendix B. **Model equations** (s, θ) **for each closure.**
∘ Quadratic Closure

$$\begin{aligned} \dot{s} \quad &= \quad 3s[N(1-s^2) - 2] + aPe(1-s^2)\sin 2\theta, \\ \dot{\theta} \quad &= \quad -\tfrac{Pe}{2}(1 - \tfrac{a}{s}\cos 2\theta), \\ s \quad &= \quad \sqrt{1 - \tfrac{2}{N}}, \\ N_*(a) \quad &= \quad \tfrac{2}{1-a^2}. \end{aligned} \tag{54}$$

∘ Tsuji-Rey Closure

$$\begin{aligned} \dot{s} \quad &= \quad \tfrac{1}{8}(3s[N(8-5s^2) - 16] + aPe(8-5s^2)\sin 2\theta), \\ \dot{\theta} \quad &= \quad -\tfrac{Pe}{2}(1 - \tfrac{a(8-s^2)}{8s}\cos 2\theta), \\ s \quad &= \quad \sqrt{\tfrac{5}{8}(1 - \tfrac{2}{N})}, \\ N_*(a) \quad &= \quad \tfrac{10+2a^2+5\sqrt{4+2a^2}}{10-4a^2}. \end{aligned} \tag{55}$$

∘ HL1 Closure

$$\begin{aligned} \dot{s} \quad &= \quad \tfrac{2}{5}(3s[N(1-s^2) - 5] + aPe(1-s^2)\sin 2\theta), \\ \dot{\theta} \quad &= \quad -\tfrac{Pe}{2}(1 - \tfrac{a(2+3s^2)}{5s}\cos 2\theta), \\ s \quad &= \quad \sqrt{1 - \tfrac{5}{N}}, \\ N_*(a) \quad &= \quad \tfrac{5-6a^2+\sqrt{25-24a^2}}{2(1-a^2)}. \end{aligned} \tag{56}$$

◦ HL2 Closure

$$\begin{aligned}\dot{s} &= 2(3s[N\{\tfrac{68}{315}e^{6+\frac{16}{s^2-3}}+\tfrac{s^2}{1+s^2}(1-s^2)\}-1]\\ &\quad +aPe[\tfrac{68}{315}e^{6+\frac{16}{s^2-3}}+\tfrac{s^2}{1+s^2}(1-s^2)]\sin 2\theta),\\ \dot{\theta} &= -\tfrac{Pe}{2}(1-\tfrac{a}{315}(136e^{6+\frac{16}{s^2-3}}+315s^2)\cos 2\theta).\end{aligned} \tag{57}$$

REFERENCES

[1] D. R. J. Chillingworth, E. Vicente Alonso and A. A. Wheeler, *Geometry and dynamics of a nematic liquid crystal in a uniform shear flow*, J. Phys., **34** (2001), 1393-1404.

[2] F. Cocchini, C. Aratari and G. Marruucci, *Tumbling of rodlike polymers in the liquid-crystalline phase under shear flow*, Macromolecules, **23** (1990), 4446-4451.

[3] E. J. Doedel *et al.*, AUTO97: Continuation and bifurcation software for ordinary diffrential equations, Concordia University (1998).

[4] M. Doi, *Molecular dynamics and rheological properties of concentrated solutions of rodlike polymers in isotropic and liquid crystalline phases*, J. Polymer Science, **19** (1981), 229-243.

[5] B. Ermentrout, *Simulations, analyzing, and animating dynamical systems: A guide to XP-PAUT for researchers and students*, SIAM (2002).

[6] V. Faraoni, M. Grosso, S. Crescitelli and P.L. Maffetone, *The rigid-rod model for nematic polymers: An analysis of the sher flow problem*, J. Rheol., **43** (1999), 829-843.

[7] J. Feng, C. V. Chaubal and L. G. Leal, *Closure approximations for the Doi theory: Which to use in simulating complex flows of liquid crystalline polymers*, J. Rheol., **42** (1998), 1095-1119.

[8] M. G. Forest and Q. Wang, *Monodomain response of finite-aspect-ratio macromolecules in shear and related linear flows*, Rheol Acta, **42** (2003), 20-46.

[9] M. G. Forest, Q. Wang and H. Zhou *Exact banded patterns from a Doi-Marrucci-Greco model of nematic liquid crystal polymers*, Phys. Rev. E, **61** (2000), 6655-6662.

[10] M. G. Forest, R. Zhou and Q. Wang, *Full-tensor alignment criteria for sheared nematic polymers*, J. Rheol., **47** (2003), 105-127.

[11] M. G. Forest, R. Zhou and Q. Wang, *Scaling behavior of kinetic orientational distributions for dilute nematic polymers in weak shear*, J. Non-Newtonian Fluid Mech., **116** (2004), 183-204.

[12] M. Golubitsky and D. G. Schaeffer, Singularities and Groups in Bifurcation Theory, Springer-Verlag (1985).

[13] S. Hess, *Fokker-Planck equation approach to flow alignment in liquid crystals*, Z. Naturforsch, **31** a (1976), 1034-1037.

[14] R. Kupferman, M. N. Kawaguchi, M. M. Denn, *Emergence of structure in a model of liquid crystalline polymers with elastic coupling*, J. Non-Newtonian Fluid Mech., **91** (2000), 255-271.

[15] Y. Kuznetsov, Elements of Applied Bifurcation Theory, Springer-Verlag (1995).

[16] N. Kuzuu and M. Doi, *Constitutive equation for nematic liquid crystals under weak velocity gradients derived from a molecular kinetic equation*, J. Phys. Soc. Japan, **52** (1983), 3486-3494.

[17] R. G. Larson and H. C. Öttinger, *Effect of molecular elasticity on out-of-plane orientations in shearing flow of liquid-crystalline polymers*, Macromolecules, **24** (1991), 6270-6282.

[18] P. L. Maffetone and S. Crescitelli, *The rigid rod model for nematic polymers: Testing closure approximations with bifurcation analysis*, J. Rheol., **38** (1994), 1559-1570.

[19] P. L. Maffetone and S. Crescitelli, *Bifurcation anaylsis of a molecular model for nematic polymers in shear flow*, J. Non-Newtonian Fluid Mech., **59** (1995), 73-91.

[20] P. L. Maffetone, M. Grosso, M. C. Friedenberg and G. G. Fuller, *Extensional flow of a two-dimensional polymer liquid crystal*, Macromolecules, **34** (1996), 8473-8478.

[21] T. Maruyama, G. G. Fuller, M. Grosso and P. L. Maffetone, *The dynamics of two dimensional polymer nematics*, J. Non-Newtonian Fluid Mech., **76** (1998), 233-247.

[22] G. Marrucci and P. L. Maffettone, *Description of the liquid crystalline phase of rodlike polymers at high shear rates*, Macromolecules, **22** (1989), 4076-4082.

[23] P. L. Maffetone and G. Marrucci, *Nematic phase of rodlike polymers. I. Predition of transient behavior at high shear rates*, J. Rheol., **34** (1990), 1217-1230.

[24] P. L. Maffetone and G. Marrucci, *A two-dimensional approach to the constitutive equation of nematic polymers*, J. Non-Newtonian Fluid Mech., **38** (1991), 273-288.

[25] H. See, M. Doi and R. Larson, *The effect of steady flow fields on the isotropic-nematic phase transition of rigid rod-like polymers*, J. Chem. Phys. **92** (1990), 792-800.
[26] S. H. Strogatz, Nonlinear Dynamics and Chaos, Westview (2000).
[27] E. Vicente Alonso, A. A. Wheeler and T. J. Sluckin, *Nonlinear dynamics of an nematic liquid crystal in the presence of a shear flow*, Pro. Roy. Soc. A, **459** (2003), 195-220.
[28] K. S. Yim, G. G. Fuller, A. Datko and C. D. Eisenbach, *Isotropic-nematic phase transitions of lyotropic, two-dimensional liquid crystalline polymer solutions*, Macromolecules, **34** (2001), 6972-6977.

Received March 2005; revised September 2005.

E-mail address: forest@amath.unc.edu